USE OF SUPERRESOLUTION ENHANCED CHRIS/PROBA IMAGES FOR LAND-COVER CLASSIFICATION AND SPECTRAL UNMIXING

J. C.-W. Chan [a, *], J. Ma [a], L. Demarchi [a], T. Van de Voorde [a], F. Canters [a]

[a] CGIS Research Group, Department of Geography, Vrije Universiteit Brussel, 1050, Brussels, Belgium - (cheuchan, jianma, ldemarch, tvdvoord, fcanters)@vub.ac.be

KEY WORDS: Superresolution, hyperspectral, CHRIS/Proba, land-cover classification, linear spectral unmixing

ABSTRACT:

CHRIS/Proba represents a new generation of hyperspectral-oriented data that provides different viewing angles of the same scene. This multi-angle acquisition, with 18 bands between 0.4-1 μm at five different angles, can substantially improve characterization of various land-cover types. However, with around 18m pixel size, the spatial resolution is still too coarse for many applications. To improve the resolution of CHRIS data, we propose the use of a superresolution (SR) image reconstruction method utilizing the information present in the multi-angle imagery. CHRIS images were first pre-processed and atmospherically corrected. Then a selected superresolution method was applied to upscale the spatial resolution to around 10m. The SR enhanced images show significant improvements in terms of contrasts and detail**.** The added value of SR imagery for land-cover classification and spectral unmixing was evaluated. In terms of classification accuracy, the use of SR CHRIS images leads to marginal increase in classification accuracies. The large amount of additional classification detail requires extended ground truth for validation. Spectral unmixing applied on SR CHRIS shows that fraction images have more detail and are more accurate than the fraction images derived from the original CHRIS images.

1. INTRODUCTION

CHRIS/Proba stands for Compact High Resolution Imaging Spectrometer onboard the Project for On-board Autonomy. CHRIS imagery is unique in its hyperspectral-oriented configuration, which provides in Mode 3 five different views of the same scene in 18 bands between 0.4 and 1 μm at 18m spatial resolution. This 18-band configuration substantially enhances the potential for land-cover mapping applications and its spatial resolution is the finest among spaceborne hyperspectral sensors. Previous studies have shown that hyperspectral data are more effective than conventional broadband multi-spectral imagery for detailed vegetation mapping at the ecotope level (Chan and Paelinckx, 2008) as well as for urban-related mapping tasks (Chan and Canters, 2007). However, even at the resolution of 18m, CHRIS data is still too coarse to be useful for many applications. Hence, it is worthwhile to investigate the possibility of upscaling the CHRIS data sets using superresolution methods in the context of land-cover classification tasks.

Superresolution refers to reconstruction methods that can be applied to obtain an image with higher spatial resolution through the use of several lower-resolution (LR) images (Park *et al.*, 2003). The idea is to achieve the best image quality possible from several LR images. However, not all LR images are useful for SR. The application of SR algorithms is possible only if the LR images are sub-sampled, meaning that aliases exist, and that the images represent sub-pixel shifts.

Closely related to the problems of image restoration and image interpolation, SR can be considered as a second generation of image restoration techniques which do not only aim at recovering a degraded image, but also at changing the image dimension using interpolation algorithms. However, the quality of a single LR image is limited and interpolation based on an under-sampled image does not allow recovering the lost high-frequency information. Hence multiple observations of the same scene are needed. The multi-angle images of CHRIS can be considered as representing several observations with degraded quality. An important step in SR is to model the relationship between the original high resolution (HR) scene and a set of LR images of the same scene. If we have N LR images and Y_k is the k^{th} LR image and the HR image is X ($\underline{X}$ and $\underline{Y_k}$ are their matrix form), then this relationship can be formulated as follows:

$$\underline{Y}_k = D_k C_k F_k \underline{X} + n_k \qquad k = 1,\ldots, N \tag{1}$$

In equation (1), F_k is the warp matrix that represents the shift and rotation of the LR images, C_k is the blur matrix that represents the blurring effects that occur during the acquisition and D_k is the subsampling or decimation factor. Lastly, n_k stands for the ordered noise vector. This model can be illustrated as a block diagram in Figure 1. Based on equation (1), different approaches have been formulated to estimate the expected high resolution images (Park *et al.*, 2003)

Superresolution image reconstruction is an active research theme and various methods have been applied to multi-angle thermal data (Galbraith *et al.*, 2005) and hyperspectral data (Akgun *et al.*, 2005). Most previous studies are based either on simulated data sets or temporal images where sub-pixel shifts occur. A problem of using temporal data sets for superresolution is that changes may have occurred in between acquisitions. In the case of CHRIS, the almost instant acquisition of five different images makes it ideal for superresolution processing in the sense that possible changes are minimized in between acquisitions. The multi-angle images acquired at nadir, ±36° and ±55° can be treated as a series of LR images of the same location where aliases exist. Recently, Chan *et al.* (2008a) studied the use of different SR methods to enhance the level of spatial detail in CHRIS images. By utilizing its multi-angular measurements, using only the nadir and the ±36° images as LR input images, the spatial resolution of CHRIS images were improved to

* Corresponding author.

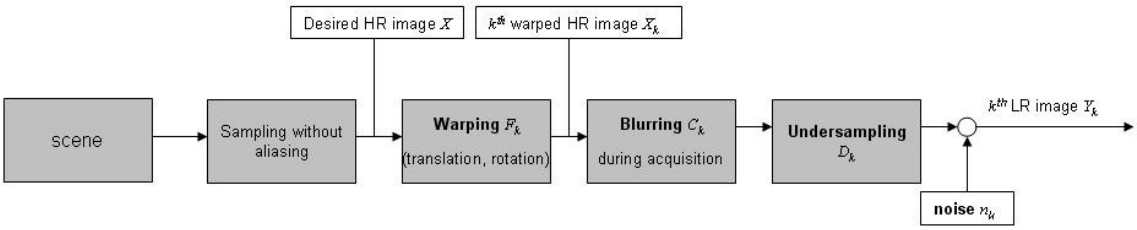

Figure 1. A flow chart showing the relationship between the desired high resolution image and the low resolution images

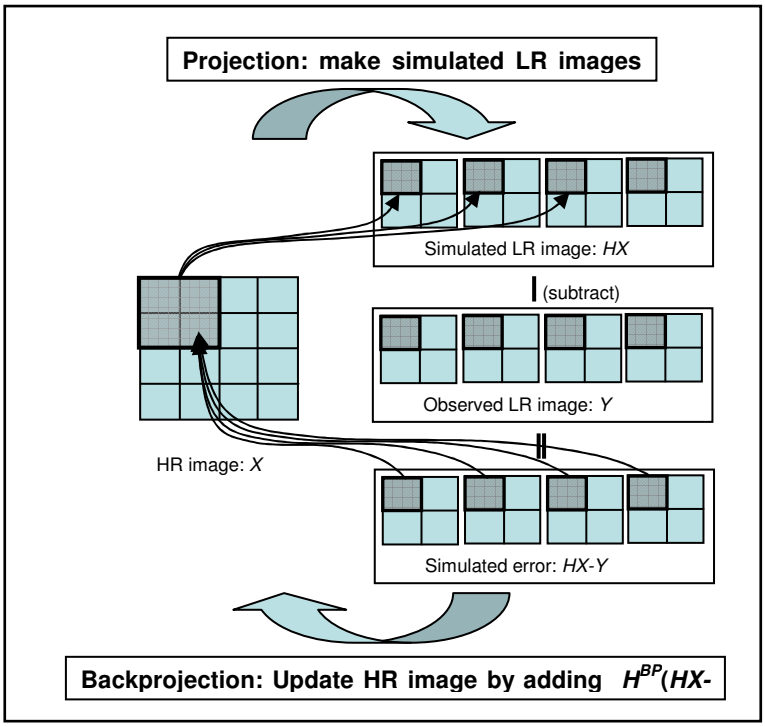

Figure 2. The Iterative Backprojection superresolution method

about 9-10m. The enhanced data sets demonstrated an interesting potential for detailed land-cover mapping at the ecotope level (Chan *et al.*, 2008b). Unlike conventional pan-sharpening methods, SR improves spatial resolution without the availability of an additional HR data set. In this paper, we present further findings concerning the use of SR enhanced CHRIS data for detailed land-cover classification as well as preliminary results from spectral unmixing.

2. METHODOLOGY

2.1 Superresolution algorithm

There are many approaches to conduct superresolution image reconstruction. First proposed in Irani and Peleg (1991), iterative backprojection (IBP) is based on a similar idea as computer-aided tomography, where a 2-D object is reconstructed from its 1-D projections. The method involves a registration procedure, an iterative refinement for displacement estimation, and a simulation of the imaging process (the blurring effect) using a point spread function.

The process starts by producing an initial guess of the HR image (Fig. 2). This initial HR image can be generated from one of the LR images by decimating the pixels. In the case of CHRIS/Proba, the nadir image sets were used as the first guess. The HR image is then down-sampled to simulate the observed LR images using the motion estimation and blurring component. The simulated LR images are subtracted from the observed LR images. If the initial HR image is the real observed HR image, then the simulated LR images and the observed LR images would be identical and their differences zero. If they are not identical, the computed differences can be "back-projected" to improve the initial guess. The back-projecting process is repeated iteratively to minimize the differences between the simulated and the observed LR images, and subsequently produce a better HR image.

The iterative procedure can be described by

$$X^{n+1} = X^n - G^{BP}(HX - Y) \tag{2}$$

where $Y = \begin{bmatrix} y_1 \\ \\ y_p \end{bmatrix}$ and $H = \begin{bmatrix} D_1 C_1 F_1 \\ \\ D_p C_p F_p \end{bmatrix}$.

G^{BP} represents the back-projection filter, X^{n+1} is the improved HR image at the $(n+1)^{th}$ iteration, and X^n is the HR image at the n^{th} iteration. IBP is intuitive, hence it is easy to understand. In this study the back-projection filter was represented by a transpose of a PSF approximated by a 7 x 7

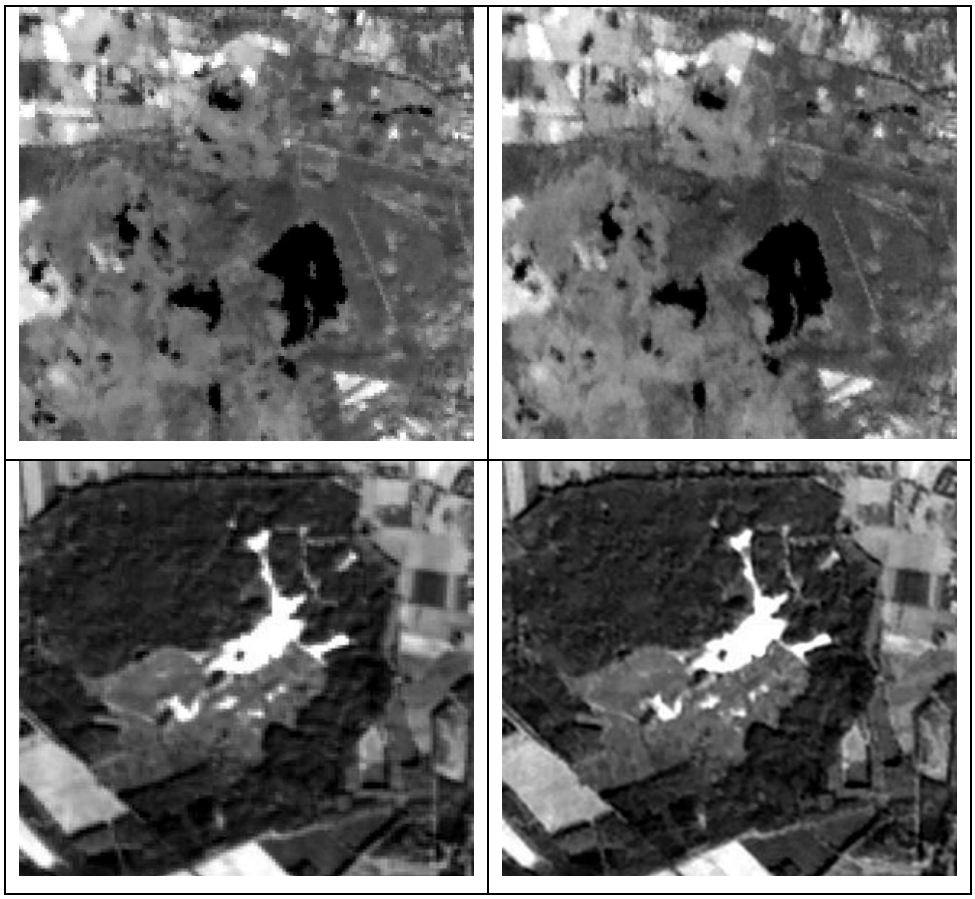

Figure 3. The original band 18 of the CHRIS nadir images (left), the SR CHRIS images using the iterative backprojection method (right) for the Kalmthout site (top) and for the Ginkelse Heide site (bottom).

kernel with variance set at 1.6. Because of the ill-posed nature of IBP, the solution it provides is not unique. The choice of the back-projection filter is decided empirically.

2.2 Data sets

Two CHRIS image sets were used in this study: (1) Kalmthout, Belgium, acquired on 1st July, 2008, and (2) Ginkelse Heide, the Netherlands, acquired on 22nd October, 2008. Both image sets are of excellent quality and cloud free. After atmospheric correction (Guanter et al., 2005), the images were co-registered and geo-referenced to the locally used map projection reference system for extraction of training samples and endmembers. The classification scheme was prepared in the context of the HABISTAT project, which focuses on mapping NATURA2000 priority land-cover types – heathland. (http://habistat.vgt.vito.be/modules/objectives/). For the Kalmthout site, there are 18 classes. The description of each class and the number of training samples are listed in Tables 1. We use the Ginkelse Heide site for the test of spectral unmixing. A set of airborne AHS data was also acquired of the Ginkel Heide site on 7th Oct., 2007. This data set was used to validate the fraction images generated from the SR CHRIS images.

3. RESULTS AND DISCUSSION

3.1 IBP superresolution enhanced images

Our initial experiments showed that using all five viewing angles does not generate satisfactory results. Hence, a SR image was produced for each of the 18 bands using only the nadir and ±36° image sets. Both image sets were considered as accurately co-registrated with the nadir images. With SR enhancement, the CHRIS images were upscaled to around 11m, doubling the original pixel resolution. Visual inspection of the SR images shows significant enhancements as compared to the original images (Fig. 3). Much additional detail is present in the SR image. The representation of boundaries between land parcels is improved. Higher contrast is observed in highly textured areas such as forest. Individual objects are better delineated and their shapes become more apparent.

3.2 Detailed land-cover classification results

A tree-based ensemble classifier Random Forest was chosen for the classification tasks. Due to the few number of training samples for certain classes, we used the out-of-bag method in the Random Forest program for validation. Out-of-bag is an objective estimation method, where the construction of each tree uses only two-third of the samples, and the remaining one-third of the samples is used for blind testing. It is a kind of cross-validation method employed in occasions where too few field training samples are available to create a separate test set. Different inputs were used: (1) nadir original image (18 bands), (2) nadir and ± 36° images (3x18=54 bands), (3) SR image (18 bands). The classification results for the Kalmthout site are shown in Table 1. The results show substantial increase in classification accuracy (≈10%) when off-nadir images are incorporated. The use of the SR image produces the highest overall accuracy (84%). Class accuracies show a substantial increase for most classes with

ID	Ecotope Classes	No. of samples in Chris/Proba	Nadir images	Nadir and ±36° images	No. of samples in SR images	SR images
1	Arable field	735	88.9	94.4	2712	93.7
2	Bare sand	84	89.7	84.5	267	96.5
3	Deciduous forest – Beech	17	33.3	0	49	81.8
	Deciduous forest – Mixed oak-birch forest	279	55.5	57.3	977	76.9
5	Coniferous forest – Scots pine	1922	84.8	96.6	7478	88.5
6	Coniferous forest – exotic conifers	186	58.8	46.8	647	94.1
7	Grassland - temporary	445	69.3	82.7	1685	83.6
8	Grassland – permanent agriculturally improved, species poor	885	75.3	91.9	3296	85.5
9	Grassland – permanent agriculturally improved, species rich	115	44.9	61.7	338	84.8
10	Grassland – permanent, semi-natural	21	0.0	23.8	65	79.2
11	Heathland – wet, open	388	61.9	85.3	1422	72.8
12	Heathland – dry, open	242	45.9	59.9	839	76.4
13	Heathland – dry, with trees	408	53.6	64.2	1439	78.6
14	Heathland – grass encroached, open, dry	451	55.8	59.2	1680	73.4
15	Heathland – grass encroached, open, wet	495	55.2	74.1	1821	74.8
16	Heathland – grass encroached, open	748	60.8	77.3	2827	73.0
17	Urban	164	94.6	94.5	536	98.7
18	Water - oligotrophic	337	99.4	99.7	1288	99.8
	Overall Accuracy		**73.2%**	**82.9%**		**84%**

Table 1. Classification accuracies for the Kalmthout site

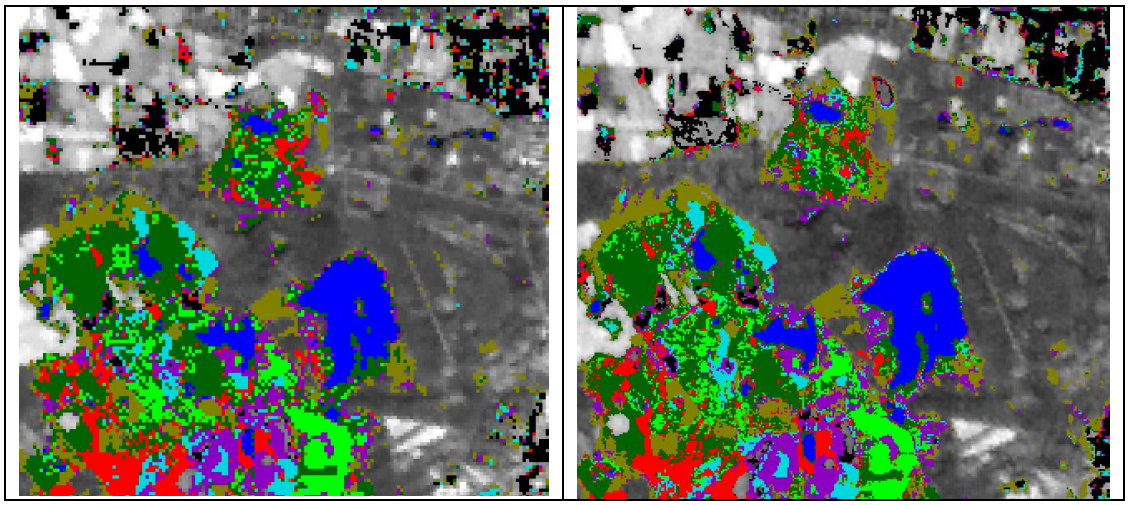

Figure 4. Detail of ecotope maps produced from the original nadir images (left) and from SR enhanced CHRIS imagery using the iterative backprojection method (right) for the Kalmthout site. The color schemes used and the descriptions of the classes are found in Table 1.

the SR approach. Classes with the least (very few) training samples seem to benefit most, e.g. classes 2, 3 and 10. Figure 4 compares the classification result generated from the original nadir CHRIS images and the SR enhanced images. The amount of detail has been substantially increased as for every original CHRIS pixel, now we have four. The higher level of spatial detail in the classification obtained with SR imagery requires more detailed validation to determine whether the extra detail represents useful, thematically correct information. Unfortunately, more detailed validation was not possible within the scope of this paper.

3.3 Spectral unmixing results

Linear spectral unmixing is a commonly accepted approach to analyze the massive volume of data provided by imaging spectrometers. Such a method applies a linear mixture model to estimate the abundance fractions of different spectral signatures within mixed pixels. The key task in linear spectral mixture analysis is to find an appropriate suite of pure spectral signatures (called 'endmembers') which are then used to model the at-sensor pixel spectra through a linear combination of endmember signatures. The model assumes that a mixed pixel is a linear combination of these endmember signatures weighted by the correspondent abundance fractions. An endmember is an idealized pure signature for a class. Endmember extraction is one of the fundamental and crucial tasks in hyperspectral data exploitation. During the last decade, several algorithms have been proposed for the purpose of autonomous/supervised endmember selection from hyperspectral scenes. An ultimate goal of an endmember extraction algorithm is to find the purest form of each spectrally distinct material in the scene. In this study we have chosen the popular pure pixel index

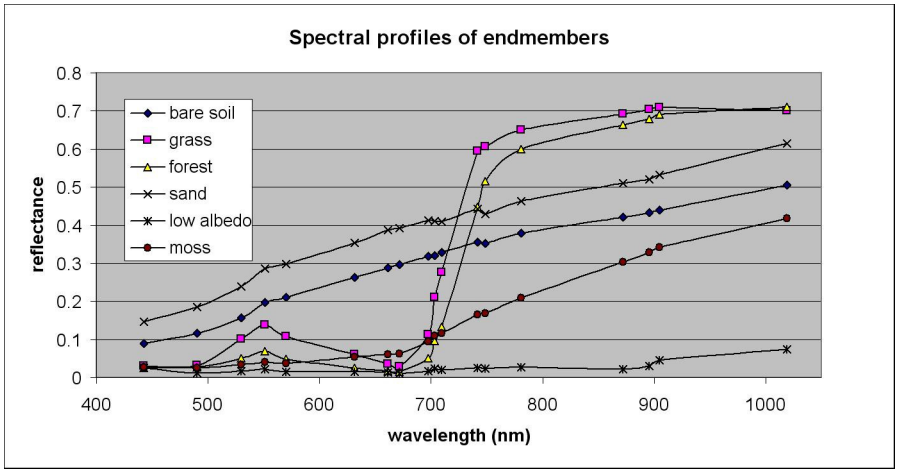

Figure 5. The spectral profiles of the six endmembers defined for spectral unmixing

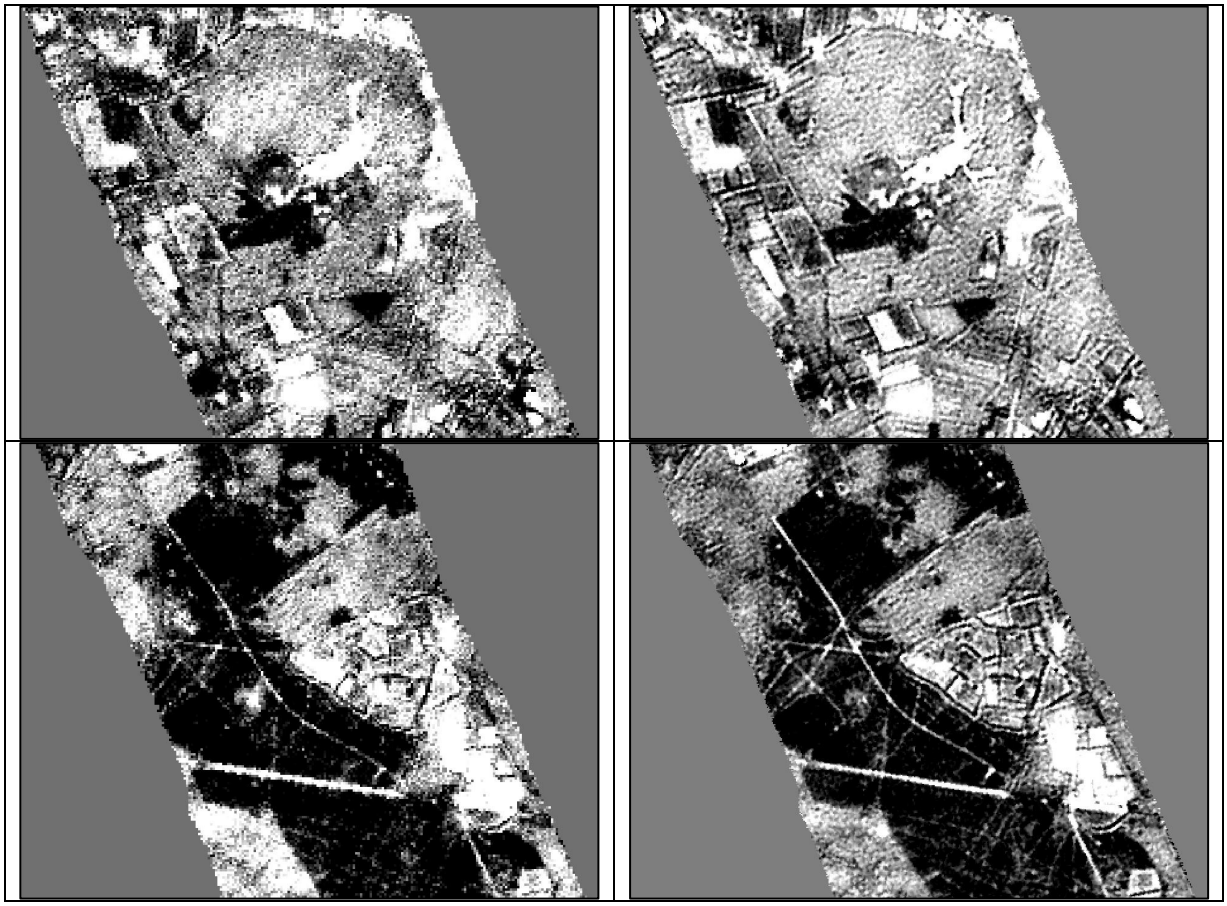

Figure 6. Fraction of sand resulting from unmixing the original CHRIS nadir images (left) and the SR enhanced CHRIS images (right).

method (Boardman et al., 1995). The six endmembers we defined for our experiments and their spectral profiles are plotted in Figure 5. Figure 6 shows the result of sub-pixel sand fractions estimated by spectrally unmixing the original image and the enhanced SR image. The difference in spatial resolution between both images is reflected clearly in the unmixing results. For validating the unmixing quantitatively, we applied a multi-resolution approach (Van de Voorde et al., 2006; Flanagan and Civco, 2001) in which a high resolution airborne hyperspectral data set is used to derive reference proportions of the sand class. An airborne AHS data set of 2.4m pixel size acquired on 7th Oct., 2007, about 2 weeks before the CHRIS acquisition, was used to create the ground truth. First, we created a binary classification of sand/non-sand from the 2.4m resolution airborne data. Because the spatial resolution of the airborne data is high compared to the coarse CHRIS original data (21m) and the SR CHRIS data (11m), we assume that the binary classification is more accurate than the unmixing results, which warrants its use as ground truth. We then randomly selected 1422 sample cells from a 42m by 42m grid containing 2 by 2 pixels of the original CHRIS image. Of the sample cells that were used for validation, 938 contained no sand and 204 were fully or partly covered by sand. The area

of each sample cell covers 3.8 by 3.8 SR CHRIS pixels and 17.5 by 17.5 AHS pixels from the binary classification. For each 42m sample cell, the sand proportion was calculated from the binary ground truth image and from the unmixed CHRIS and SR CHRIS sand fraction images. The following error measure was used to assess the accuracy of the sub-pixel proportion estimates on the validation set:

$$MAE_{sand} = \frac{\sum_{i=1}^{N} | P_i^{'} - P_i |}{N} \quad (3)$$

With

N : the total number of pixels in the validation sample

P_i : the proportion of sand inside validation cell i, derived from the binary classification obtained with the high resolution airborne data (ground truth)

P'_i: the proportion of sand inside validation cell i, estimated by spectral unmixing

The mean absolute error MAE_{sand} quantifies the error magnitude and can be interpreted as a mean error percentage. The sand fractions estimated by spectrally unmixing the CHRIS and SR CHRIS data have an MAE_{sand} of 0.0899 and 0.0674, respectively. This indicates that proportions predicted from the SR images are more accurate.

4. CONCLUSIONS

The multi-angle property of CHRIS/Proba image sets enables the use of superresolution image reconstruction. Based on previous studies SR CHRIS images were generated with the IBP method. Significant improvements in terms of level of detail and image contrast are observed with the SR CHRIS images, as the spatial resolution is increased to around 10m. The SR CHRIS images were used for land-cover classification and for spectral unmixing in heathland area.

Accuracy assessments carried out in this study show that the use of SR CHRIS marginally increases classification accuracy. Results of spectral unmixing show that the SR CHRIS data produce more accurate results and substantially more detail. Since the classification or fraction maps are provided in higher spatial resolution (the number of pixels was quadrupled), more validation efforts with spatially detailed ground truth are required to verify the preliminary results obtained in this study. We believe SR image reconstruction may substantially increase the application potential of standard multi-angle CHRIS/Proba imagery.

Acknowledgements

The research presented in this paper is partially funded by the Belgian Science Policy Office in the frame of the STEREO II programme - project HABISTAT (SR/00/103) and by the Vrije Universiteit Brussel in the frame of the HOA Project HYPERENV (HOA19). The authors wish to thank Alterra of Wageningen University and INBO (Research Institute for Nature and Forest – scientific institute of the Flemish Government) for providing the ground truth for the classification experiments in this study.

References

Akgun, T., Altunubasak, Y., and Mersereau, R.M., 2005. Super-resolution reconstruction of hyperspectral images. *IEEE Trans. Geosci. and Remote Sensing*, 14, pp.1860-1875, 2005.

Boardman, J.W., Kruse, F.A., and Green, R.O., 1995. Mapping target signatures via partial unmixing of AVIRIS data. In *Proc. Summaries JPL Airborne Earth Science Workshop*, Pasadena, CA, 1995, pp.23-26

Chan, J.C.-W., Ma, J. and Canters, F., 2008a. A comparison of superresolution reconstruction methods for multi-angle Chris/Proba images. *Proceedings of SPIE Image and Signal Processing of Remote Sensing XIV*, September 15-18, 2008, University of Wales Institute, Cardiff, Wales, United Kingdom. 7109(710904), pp 1-11. DOI: 10.1117/12.800256.

Chan, J.C.-W., Ma, J., Kempeneers, P., Canters, F., Vandenborre, J. and Paelinckx, D., 2008b. An evaluation of ecotope classification using superresolution images derived from Chris/Proba data. *Proceedings of IGARSS*, July 6-11, 2008, Boston, Massachusetts, USA. Vol. III, pp 322-325.

Chan, J.C-W and Canters, F., 2007. Ensemble classifiers for hyperspectral classification. On CD-ROM, *Proceedings of the 5th EARSeL SIG IS*, Innovation in Environmental Research (Bruges 23-25 April).

Chan, J.C-W and Paelinckx, D., 2008. Evaluation of Random Forest and Adaboost tree-based ensemble classification and spectral band selection for ecotope mapping using airborne hyperspectral imagery. *Remote Sensing of Environment*, 112, 2999-3011.

Flanagan, M. and Civco, D.L., 2001. Subpixel impervious surface mapping. In *Proceedings of the ASPRS 2001 Annual Conference, 23-27 April, St. Louis, MO*. (Bethesda, Maryland: American Society for Photogrammetry and Remote Sensing), unpaginated CD-ROM.

Galbraith, A., Theiler, J., Thome, K., and Ziolkowski, R., 2005. Resolution enhancement of multi-look imagery for the multispectral thermal imager. *IEEE Trans. Geosci. and Remote Sensing*, 43, pp.1964-1977, 2005.

Guanter, L. Alonso, L., and Moreno, J., 2005a. A method for the surface reflectance retrieval from PROBA/CHRIS data over land: application to ESA SPARC campaigns. *IEEE Transactions on Geoscience and Remote Sensing*, 43, pp. 2908-2917, 2005.

Irani, M., and Peleg, S., 1991. Improving resolution by image registration [J]. *CVGIP: Graphical Models and Image Proc*., 53(5), pp. 231-239, 1991.

Park, S.C., M.K. Park, and Kang, M.G., 2003. Super-resolution image reconstruction: A technical overview. *IEEE Signal Process. Mag*., 20(3), pp. 21-36.

Van de Voorde, T., De Genst, V., and Canters, F., 2006. Sub-pixel mapping of impervious surfaces from Landsat ETM+ data using reference proportions derived from VHR data. In *Proceedings of the 25th EARSeL symposium - Global Developments in Environmental Earth Observation from Space*, D. Marcal (ed.), pp. 547-555.